Tuning Gold Nanoparticle Self-Assembly for Optimum Coherent Anti-Stokes Raman Scattering and Second Harmonic Generation Response

Christopher J. Addison,[†,‡] Stanislav O. Konorov,[†,‡] Alexandre G. Brolo,*[,§] Michael W. Blades,[†] and Robin F.B. Turner*[,†,‡,∥]

Department of Chemistry, The University of British Columbia, 2036 Main Mall, Vancouver, BC, Canada, V6T 1Z1, Michael Smith Laboratories, The University of British Columbia, 2185 East Mall, Vancouver, BC, Canada, V6T 1Z4, Department of Chemistry, University of Victoria, PO Box 3065, Victoria, BC, Canada, V8W 3V6, and Department of Electrical and Computer Engineering, The University of British Columbia, 2332 Main Mall, Vancouver, BC, Canada, V6T 1Z4

Received: October 29, 2008; Revised Manuscript Received: January 1, 2009

The research and development of new substrates for use in surface-enhanced spectroscopy is primarily motivated by the ability to tune such substrates to provide maximum signal enhancement and therefore lower detection limits. We examined a series of multilayer nanoparticle (NP) arrays with between 1 and 17 NP layers using two nonlinear optical (NLO) techniques: Coherent anti-Stokes Raman scattering (CARS) and second harmonic generation (SHG). The CARS signal of oxazine 720 was monitored at 1600 cm^{-1} using a 709-nm pump beam and an 800-nm stokes beam. Maximum signal was observed for 11 NP layers and is attributed to the matching of the CARS signal and the substrate surface plasmon excitation at 637 nm. The CARS signal for the 3000-cm^{-1} C−H stretching vibration showed maximum enhancement at 13 NP layers. The maximum SHG signal enhancement occurred at 13 NP layers, with a 50-fold overall enhancement of the SHG signal. We demonstrate that the NP-containing substrates can be tuned to provide maximum NLO response based on the number of NP depositions and the wavelength(s) involved in the NLO experiments. These multilayer NP arrays yield a stable and modular spectroscopic substrate advantageous for a variety of surface-enhanced spectroscopic techniques.

Introduction

The study of the optical characteristics of nanostructures is among the most active branches of research in nanotechnology. The efforts in this area are driven by the prospect of important applications in biomedical imaging,[1] telecommunications,[2] optoelectronics,[3] and photonics.[4] Metallic nanostructures are particularly interesting, since useful optical effects may be observed in these systems due to the excitation of surface plasmon (SP) resonances. Surface-enhanced Raman scattering (SERS)[5−9] is the most studied of the SP-assisted optical effects because it can yield an average increase in signal intensities on the order of 10^4-10^6 over conventional Raman scattering. SERS has already been proven to be extremely useful in bioanalytical chemistry for the detection of submonolayer adsorbate quantities[10−12]and single molecules[13] of analytes. The surface-enhanced version of other spectroscopic methods, such as infrared absorption[14] and fluorescence,[15] has also been demonstrated. The surface-enhanced phenomenon is predicted to have a particularly important impact in nonlinear optical (NLO) applications, since the generally weak nonlinear effects can be significantly increased via strong electromagnetic (plasmon) fields at the surfaces of metallic nanostructures.[16,17] Hence, a variety of NLO effects, including second-harmonic generation (SHG),[18−20] third harmonic generation (THG),[21,22] coherent anti-Stokes Raman scattering (CARS),[23,24] two-photon photoluminescence,[25] and white light supercontinuum generation,[25] have been shown to benefit from the SP-assisted enhancement enabled by metallic nanostructures.

A major focus of research in the field of surface-enhanced spectroscopy is on the development of high-quality, reproducible, and highly enhancing nanostructures.[26] In fact, the efficiency of the enhancement can be controlled by the nature of the metal as well as geometric parameters of the nanostructures such as interparticle spacing[27−29] and aspect ratio.[30] These parameters are routinely exploited in the development of a variety of substrates for surface-enhanced linear and nonlinear spectroscopy. For example, random aggregates of nanoparticles[12,20,31] to organized arrays of particles[32,33] or holes[34] have been shown to offer varying degrees of enhancement. Particularly in the case of surface-enhanced SHG, there has been a significant amount of work on the use of organized arrays of asymmetric particles to break the centro-symmetry of the system.[33,35−37] We have previously explored the application of gold nanoparticles (Au NPs) immobilized on glass slides as substrates for SERS.[38] These substrates were created by initially derivatizing a glass microscope slide with 3-mercaptopropyltrimethoxysilane (MPTMS). The silane undergoes a condensation reaction with the glass surface to yield a pendant thiol group. The derivatized glass slides were immersed in solutions of Au NPs, which were irreversibly attached to the glass slide using the well-known gold-thiol chemistry[39] (Scheme 1). Additional Au NP layers were added by derivatization with a propanedithiol linker molecule followed by subsequent immersion in the Au NP solution. This process was repeated until the desired number of Au NP layers was produced. It was shown that these nanoparticle-containing structures have tunable optical properties

* To whom correspondence should be addressed. E-mail: agbrolo@uvic.ca (A.G.B.); turner@msl.ubc.ca (R.F.B.T.)
[†] Department of Chemistry, The University of British Columbia.
[‡] Michael Smith Laboratories, The University of British Columbia.
[§] University of Victoria.
[∥] Department of Electrical and Computer Engineering, The University of British Columbia.

10.1021/jp809579b CCC: $40.75
Published on Web 02/11/2009

SCHEME 1: Schematic Showing the Construction of the Nanoparticle Substrates Using the Alternate Immersion of Solutions of Gold Nanoparticles and a Dithiol Linker Molecule

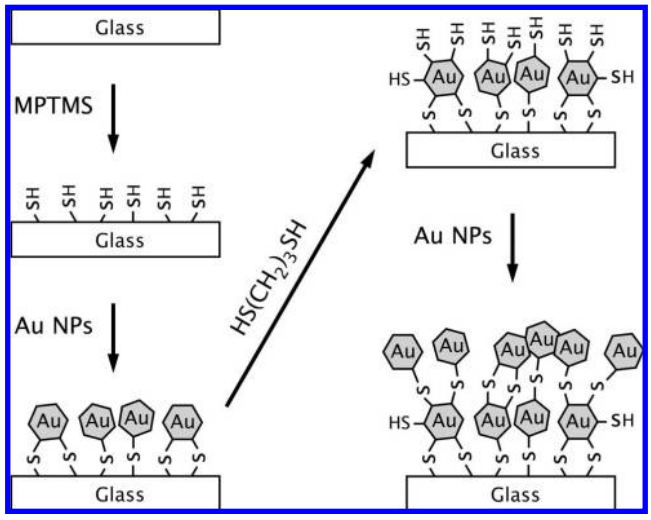

based on the number of Au NP layers that resulted.[38] Consequently, we were able to tune the number of Au NP depositions to obtain the optimum SERS effect from a probe molecule. The optimum number of Au NP depositions was dependent on the excitation wavelength, consistent with the fact that different morphologies lead to different optimal conditions for SP-excitation. Similar results were observed for nanoparticles immobilized on Au films.[40]

In this work, we show that the enhancement factor offered by Au NP layers deposited on glass can also be tailored to optimize NLO effects. Two nonlinear methods, SHG and CARS, were explored. In both cases, the increase in the efficiency of the nonlinear effect was attributed to an increase in the local field due to SP excitations at frequencies that match at least one of the fields involved in the nonlinear phenomenon.

Experimental Section

NP Substrate Synthesis and Characterization. The synthesis of the NP substrates has been described previously.[38] A diagram of the process is presented in Scheme 1. Briefly, microscope slides were derivatized by immersion in a solution of MPTMS for 12 h and then rinsed with methanol and then water. The derivatized slides were then immersed in a solution of Au NPs for 24 h to allow for complete deposition of a single Au NP layer. The Au NPs are (14 ± 2) nm in diameter and exhibit a plasmon maximum at 520 nm.[38] To add further layers of Au NPs, the substrates were immersed in a solution of the bifunctional propanedithiol (PDT) linker molecule for 15 min and rinsed with methanol and then water. Substrates were then placed in a Au NP solution for 1 h for deposition. This process was repeated until the desired number of Au NP layers had been deposited onto the substrate. For SE-CARS experiments, a methanolic solution of oxazine 720 was deposited on the top of the substrate's surface and evaporated to dryness, and excess oxazine was removed by rinsing with water.[38]

Substrates were characterized using a ThermoMicroscopes Digital AFM instrument in noncontact mode. ThermoMicroscopes I-type geometry noncontact Silicon tips (Model 1650−00), with a 120 μm length, 26−28 μm length, and 3.6−4.4 μm width were employed. Scans were of a 1000 × 1000 nm area, with a total of 200 lines scanned at 1000 nm/s.

Characterization of the substrates using UV−vis spectroscopy has been previously employed.[38] The substrates demonstrated a red-shift in the plasmon resonance band with increasing number of NP depositions.

SHG. A schematic of the SHG used in this experiment is presented in Figure 1a. Optical SHG from the nanostructured surfaces was obtained using an external reflection geometry with a 45° angle of incidence. The laser system consisted of a Coherent Innova 400 Ar+ ion pump laser and a Coherent Mira 900 F Ti:Sapphire oscillator operating at 76 MHz. The pulse repetition rate was reduced to ca. 5 MHz, using a pulse-picker system (Coherent Model 9200). The excitation wavelength was 820 nm; the nominal pulse duration was 200 fs; the pulse energy was 10 nJ. Both p- and s-polarized incident radiation was used. However the s-polarized radiation provided a very weak SH signal, and only the p-polarized experiments will be presented here. The power density at the fundamental wavelength at the sample was of the order of 5 MW cm^{-2}, and the excitation beam was focused to ca. 200 μm. This power density is below the typical damage threshold for metallic surfaces, and no indication of laser-induced surface degradation was observed. Samples were manually translated such that different portions of the substrate were used for SH experiments. In such cases, SH signal variability was on the order of 5%. The second harmonic (SH) radiation was selected using a $CuSO_4$ filter and detected using a thermoelectric cooled photomultiplier tube (PMT). Additional details on the experimental setup used for SHG can be found in a previous publication.[41]

CARS. A schematic of the CARS apparatus used in this work is shown in Figure 1b. Excitation pulses are generated by a Ti: sapphire laser system consisting of an oscillator (Mai Tai; SpectraPhysics, USA) and amplifier (Spitfire HPR; SpectraPhysics, USA). The pulses were of 150-fs duration with a total energy of 2 mJ per pulse, 1 kHz repetition rate, and 800 nm central emission wavelength. The primary laser beam was split into two secondary beams where one was used for pump and probe radiation with energy variable between 5 and 30 nJ and the other to pump the optical parametric amplifier (OPA) (Topas; Light Conversion, Lithuania), with wavelength tunability from 370 nm to 2.8 μm, to generate the Stokes, pump, or probe radiation as required.

The Stokes and pump beams are combined in a collinear geometry using a dichroic mirror and focused onto the surface with a 25-cm lens. NP samples were affixed to a two-dimensional translation stage. Samples were translated transverse to the direction of the pump beams with a lateral accuracy of 5 μm. The incident beams and anti-Stokes signal reflect from the sample surface and are collimated using a 15-cm lens before passing through a low pass dielectric filter to reject the incident beams. The anti-Stokes signal is isolated using a 150-mm focal length monochromator (SectraPro-150, Acton Research Corporation, Acton MA) prior to reaching the PMT (H5783-20, Hamamatsu, Bridgewater NJ) connected to a boxcar averager (Stanford Research Systems).

To account for any sample inhomogeneities the samples were raster scanned over the entire sample surface at an interval of 1 mm, and the CARS signal was obtained at each location. The CARS intensity at each location is an average of 3000 laser pulses (total acquisition time of 3 s), and the CARS signal presented for each sample is the average of all signals obtained over all scan locations.

Two different vibrational bands of oxazine 720 were studied in the CARS experiments. In case 1, the 1600-cm^{-1} vibration frequency (ω_{CARS} = 637 nm) attributed to the alkene stretches

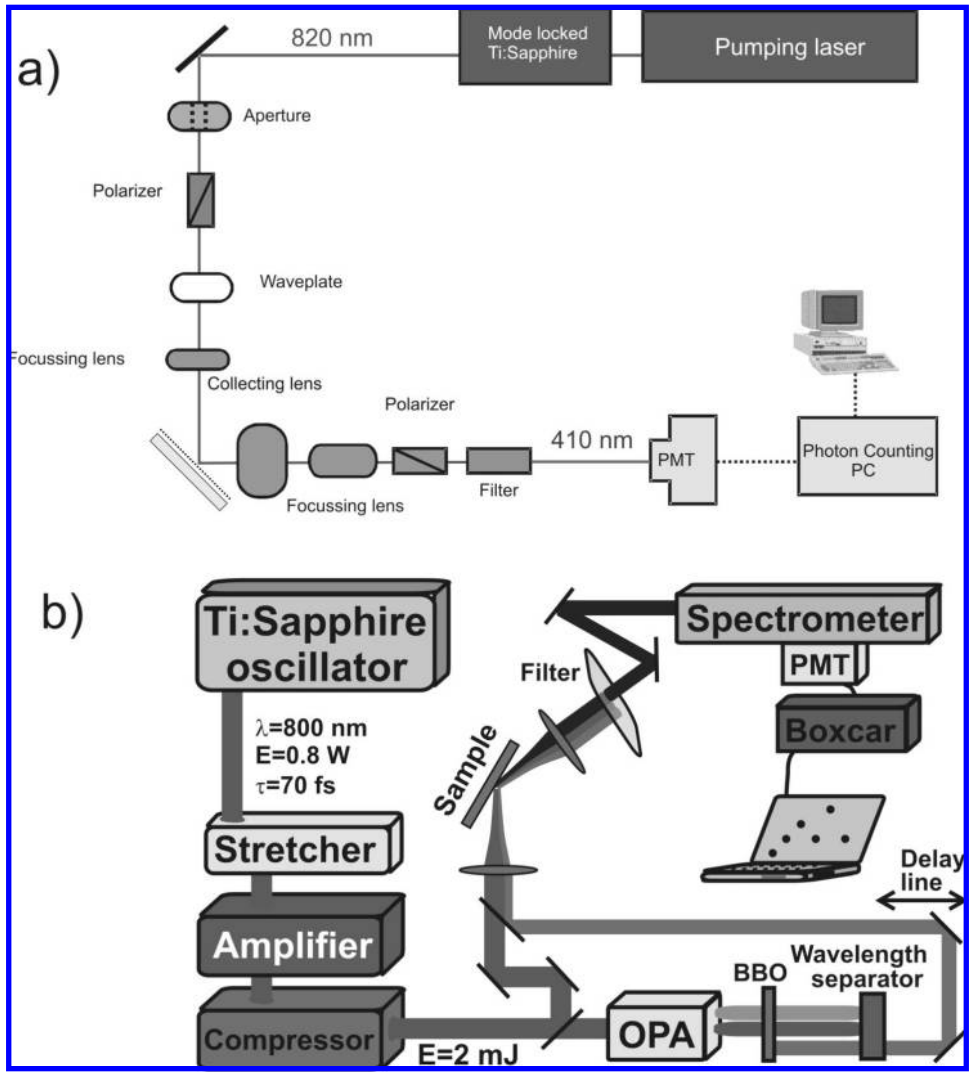

Figure 1. (a)SHG apparatus used in this work. The excitation source consisted of a mode locked Ti:Saphire laser operating at 820 nm with a 200 fs pulse duration, 10 nJ pulse energy, and a 5 MHz repetition rate. The power density is on the order of 5 MW cm^{-2}, and p-polarized incident radiation was used. (b) CARS apparatus used in this experiment. Excitation pulses were 150-fs duration with a total energy of 2 mJ per pulse, 1 kHz repetition rate, and 800 nm central emission wavelength. One portion of the laser beam was used as a pump/probe radiation with energies between 5 and 30 nJ. The other portion of the beam was used to pump the optical parametric amplifier. For 1600-cm^{-1} signal observation (ω_{CARS} = 637 nm), ω_1 = 709 nm and ω_2 = 800 nm. For 3000-cm^{-1} signal observation (ω_{CARS} = 645 nm), ω_1 = 800 nm and ω_2 = 1053 nm.

of oxazine was measured; this corresponds to pump/probe and Stokes beams of 709 and 800 nm, respectively. In case 2, the CARS signal due to the C−H stretch was monitored at 3000 cm^{-1} (ω_{CARS} = 645 nm); this corresponds to pump/probe and Stokes beams at 800 and 1053 nm, respectively.

Results and Discussion

Substrate Characterization. AFM imaging allows for the precise determination of nanometer-scale aggregate structures which are principally responsible for the generation of enhanced spectroscopic signals in NP-containing systems.[42−45] A selection of AFM images obtained from these substrates is presented in Figure 2.

With a single NP layer deposited onto the glass slide (Figure 2a), the AFM image demonstrates localized, individual NPs deposited throughout. The line scan shows vertical features, ca. 11 nm, which are on the order of the size of the NPs used in this work. Lateral distances measured in the line scans will not be accurate due to tip−sample convolution.[46]

As additional NP layers are added to the substrates the features transition to aggregatelike structures with a concomitant increase in the height and span of the features observed by AFM (parts b and c of Figure 2). This is followed by a continuous red-shift in the UV−vis spectrum,[38] which is also indicative of NP aggregation.

SH Generation. The SH signal was measured for substrates with different numbers of Au NP deposition steps, and representative data is provided in Figure 3. As exemplified in Figure 3, a substrate with a monolayer of Au NPs generates very little SH signal—on the order of 350 counts per second (cps). When a substrate with 3 Au NP depositions was tested, a much greater SH signal (near 10000 cps) was obtained, but 5−11 Au NPs deposition steps results in a decrease in the SH signal to the 1500−3000 cps range. Upon further deposition steps, the SH signal increases again to a maximum of 19000 cps obtained for 13 Au NP depositions. Substrates prepared with 15 and 17 Au NP layers yield SH signals of 6500 and 3500 cps, respectively. The absolute standard deviation in the SH measurements over multiple acquisitions from multiple samples and differing sample areas is estimated at approximately ± 20% of the measured signal. This is due to the large variations in NP properties from sample to sample and from area to area

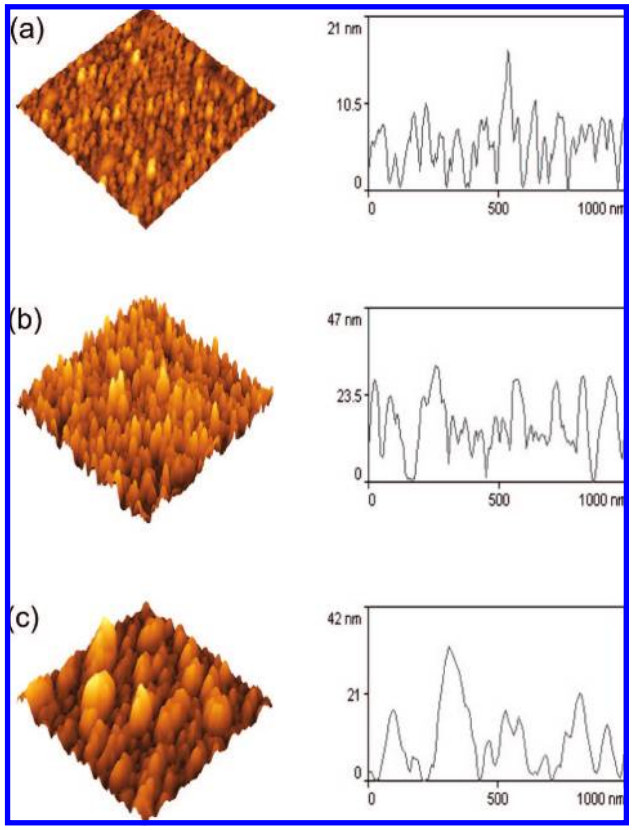

Figure 2. AFM data of multilayer nanoparticle substrates. Topograhic images (left panel) of representative areas 1000 nm × 1000 nm and representative line scans (right panel) for (a) 1, (b) 7, and (c) 15 NP depositions showing the relative vertical scale.

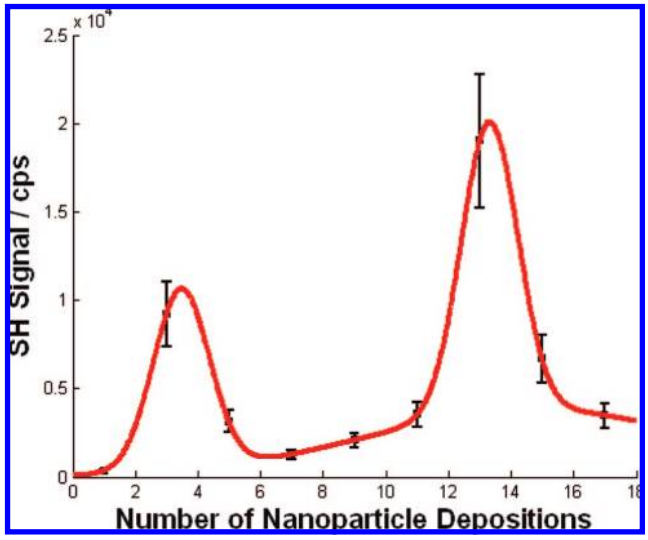

Figure 3. SHG signal of NP-containing substrates obtained using 820 nm fundamental radiation with 200 fs pulse duration and 10 nJ pulse energy at a 5 MHz repetition rate. Data was collected at a 45° incidence angle. p-Polarized radiation was used exclusively for the fundamental and the second harmonic. The maximum SHG signal is observed for 13 NP depositions.

within a sample, as commonly seen with NP systems, but in all instances the same general shape of the SH response curve was observed.

Figure 3 also shows that the two resonances occurring at 3 and 13 colloid layers superimposed on an (approximately) linearly increasing baseline. The linear increase in the background can be attributed to an increase in both the amount of deposited metal and in the surface roughness, which was shown to be directly proportional to the number of Au NP depositions.[38] Symmetry factors have previously been shown to greatly affect SHG from metallic nanostructures,[47] whereby SHG from nanostructured substrate was attributed to be principally from increasing asymmetry of the nanostructures and not from the nanogap size of the nanostructures. This may provide an additional contribution to the increasing background with the number of Au NP deposition steps.

The substrate prepared with one Au NP deposition presents very little SHG signal because the quasispherical Au NPs form a monolayer on the modified glass slide and present an UV−vis absorption characteristic of the isolated NPs.[38] Such isolated Au NPs generally exhibit a high degree of centrosymmetry, leading to a weak SHG signal.[48] With the deposition of more Au NPs, a significant increase in the SH signal should be expected due to a decrease in the overall symmetry[47] of the nanoparticle aggregates, and this is indeed what is observed, as illustrated in Figure 3.

The presence of two maxima in Figure 3 is an interesting result, suggesting that two resonance conditions were matched by the nanostructures. The SHG signal from Au NPs deposited on glass is enhanced through the same mechanism that underlies the field-enhancement in SERS.[49,50] That is to say, optical excitation of roughened surfaces results in localized SP modes and extremely large electric fields localized near certain features, such as sharp tips and nanogaps.[51] The SH signal from noncentrosymmetric systems is dominated by the dipolar response. However, quadrupolar contributions may become significant[52] as the average size of the metallic nanofeatures increase, leading to further enhanced SH generation. In our case, the feature size scales with the number of Au NP deposition steps and the quadrupolar response should thus become more important for larger Au NP depositions. The multipolar contribution has been shown to be of the order of 20% of the total SHG signal for arrays of Au nanoparticles.[53−55]

In surface-enhanced SHG, the local field enhancement (η) can be active upon the incident excitation beam (at angular frequency ω) and the harmonic field (at frequency 2ω), as given by[49]

$$\eta = |L^2(\omega)L(2\omega)| \quad (1)$$

where $L^2(\omega)$ and $L(2\omega)$ are the local fields at the excitation and at the SH frequencies, respectively. SP excitations at both the excitation and the SH fields have been observed for vapor deposited gold and silver nanostructures[50] and for metallic nanorods.[56] Therefore, a simple explanation for the two maxima in Figure 3 is that they correspond to the conditions where the morphology of the substrates allows a match between SP resonances with either the incident or the harmonic field. In this case, the origin of the maximum at 3 Au NPs deposition could be assigned to a SP resonance at the 410 nm second harmonic field which is evidently blue-shifted relative to the Au intraband transition at ~500 nm.[57] In our previous work,[38] maximum SERS were observed for 9 and 13 Au NP depositions for excitations at 633 and 785 nm, respectively. The second maximum in SH enhancement in Figure 3 is for 13 Au NP depositions which should correspond to a SP resonance at 820 nm (fundamental field), agreeing well with the previous SERS data.[38]

CARS. CARS consists of a pump beam and a Stokes beam of frequencies ω_1 and ω_2, respectively.[58] Generally, the pump beam is also used as a coincident probe beam with frequency ω_1. The anti-Stokes signal, of frequency ω_{CARS}, is generated

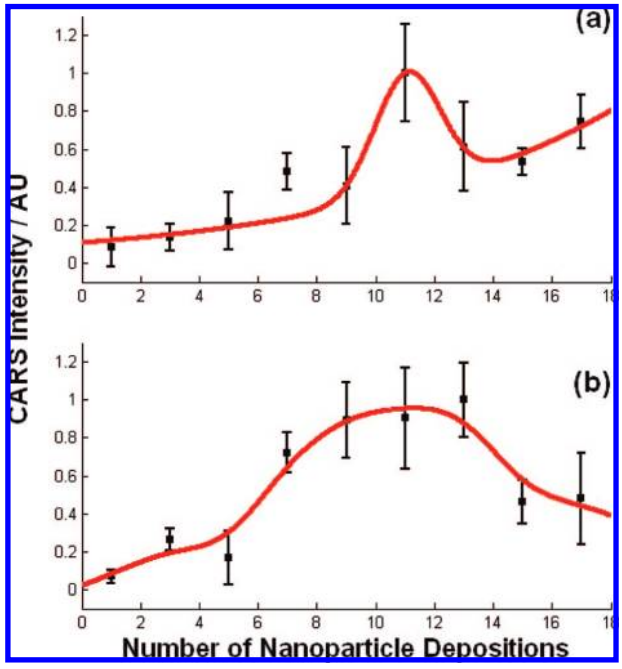

Figure 4. CARS signal of oxazine vibration with increasing number of NP depositions on the underlying substrate (a) 1600-cm^{-1} vibration (ω_{CARS} = 637 nm). Pump/probe and Stokes beams of 709 and 800 nm were used, respectively. The maximum CARS signal is observed for 11 NP depositions. (b) 3000-cm^{-1} vibration (ω_{CARS} = 645 nm). Pump/probe and Stokes beams at 800 and 1053 nm were used. The maximum CARS signal is observed for 13 NP depositions. All data collected in a collinear geometry with p-polarized radiation.

when the Raman vibration at $\omega_1 - \omega_2$. is resonantly driven by the pump and Stokes beams, yielding $\omega_{CARS} = 2\omega_1 - \omega_2$. The use of two excitation frequencies can allow for the simultaneous enhancement of local fields at both incident frequencies (ω_1, ω_2), as well as the anti-Stokes (ω_{CARS}) frequency, yielding up to four coupled fields[59] in surface-enhanced CARS (SE-CARS). The possibility of such concomitant enhancement could yield extremely high CARS signals and may thus allow for the acquisition of useful CARS signals from molecules with small nonlinear susceptibilities.

One of the first experimental reports involving SE-CARS occurred when several organic solvents were mixed with silver colloids to yield an enhanced CARS signal from the organic solvents (in a manner analogous to early SERS-based substrates).[60] Alternatively, individual, isolated gold nanoparticles (NPs) were deposited onto a derivatized gold surface to yield a substrate that is highly enhancing and where the SE-CARS signal from each particle is well localized.[23,61] In addition, SE-CARS can be implemented in a scanning mode using a metallic nanoprobe tip that can yield SE-CARS signals with high spatial resolution beyond the diffraction limit of light.[23] While these methods do yield enhancement of the CARS signal, the optical properties of the gold nanoparticles are constant and thus, in order to observe an enhanced CARS signal, the surface plasmon excitation frequency of the Au NPs must directly coincide with either one of the excitation beam(s) or the resultant anti-Stokes signal.

The results for case 1 (1600-cm^{-1} signal observation) are shown in Figure 4a. There is a slow but continuous increase in CARS intensity with increasing Au NP depositions between 1 and 9 layers. With 11 Au NP depositions, there is a dramatic increase in CARS intensity before falling to a near-constant level between 13 and 17 Au NP depositions. Maximum CARS enhancement is observed with 11 Au NP depositions, indicating that this substrate is most suitable for use with these excitation and signal frequencies. In this case, the surface-enhancement yields a modest 10-fold increase in the oxazine CARS signal. The three photons involved in the CARS process (pump, Stokes, and anti-Stokes) will all provide a contribution to the enhancement of the CARS signal when the optical properties of the Au NP containing substrates coincides with the frequency of the pump/probe, Stokes, or anti-Stokes beams. Thus, the enhanced CARS signal can be thought of as resulting from the superposition of two overlapping enhancement processes:

(i) The contributions of the pump/probe and Stokes beams to the CARS signal enhancement will increase as Au NP absorption increases at those wavelengths (709 and 800 nm).

(ii) An increase in the CARS signal enhancement should also be observed as the anti-Stokes shifted signal wavelength approaches the SP resonance condition.

For process i, the two excitation frequencies (709 and 800 nm), coincide with the overall broad red-shifted absorption associated with aggregation of the Au NPs in the substrate[26,29,62−64] for large numbers of depositions. The optical absorption of the substrate (measured by UV−vis spectroscopy) thus continuously increases with increasing Au NPs additions.[38]

For process ii, one must examine how the optical properties of the substrate physically relate to the CARS signal at 637 nm. This is not straightforward since the local fields are involved in the enhancement and the frequency of optimum SP resonance (ω_{SP}) do not always coincide with the maximum in the absorption spectrum. There are three regimes that must be considered: (1) when $\omega_{CARS} < \omega_{SP}$, increasing CARS signal will be observed as ω_{SP} moves toward ω_{CARS}; (2) maximum enhancement will be observed when $\omega_{SP} = \omega_{CARS}$; (3) enhancement decreases as ω_{SP} becomes red-shifted away from ω_{CARS}.[65,66] These regimes are reflected in the CARS response of the substrates with increasing Au NPs depositions. The maximum CARS signal at 11 NP layers is attributed to a resonance between the wavelength of the CARS signal and the localized SP resonance (at the frequency of the CARS field). As with SERS, we believe that the vast majority of the enhanced CARS signal can be attributed to a small proportion of certain nanofeatures within the substrate. These "hot spots" generate a large, localized electromagnetic field, leading to the greatest contribution to the enhancement of the CARS signal. Indeed, Etchegoin et al. previously showed that the optical properties (resonances) of these "hot spots" do not correlate with the distribution of plasmon resonances measured by UV−vis spectroscopy.[67,68] Because our CARS results were averaged over the surface of the substrate, the high intensity generated by the "hot spots" will be averaged with the low-intensity CARS signal of the underlying substrate. Further high-resolution mapping experiments could allow for the elucidation of specific "hot spot" locations and the extent of their enhancement.

Previous studies on the application of these substrates for SERS demonstrated that maximum SERS enhancement with 632.8 nm excitation was observed at 9 NP depositions.[38] The increase to 11 Au NP layers for maximum CARS enhancement observed here can be attributed to the higher CARS signal wavelength (637 nm) as well as contributions from the resonance conditions relating to the pump/probe and Stokes beams.

The results for case 2 (3000-cm^{-1} signal observation) should be very similar to case 1 (1600-cm^{-1} signal observation). The major difference is that the Stokes field lies at 1053 nm, which will be far removed from any resonance of the substrates and therefore should yield little or no enhancement of the CARS

signal. Therefore, enhancement can only be provided from process (i); i.e., from the pump beam (800 nm) or the emitted anti-Stokes signal (645 nm). The maximum CARS signal is observed in the region of 11−13 NP depositions from Figure 4b. We attribute this to increasing enhancement from the pump/probe beam, and the maximum enhancement near 13 Au NP depositions to be due to the overlap between the anti-Stokes signal and the absorption feature of the Au NP substrates. The 645-nm emitted CARS signal falls within the range (666 ± 25 nm) of the absorption maximum for the substrates determined by UV−vis spectrophotometry.

Differences between the CARS response profiles of parts a and b of Figure 3 may also be attributed in part to an unwanted CARS signal contribution from the dithiol linker molecule. That is, because of the broadband femtosecond pulses used in this experiment, the spectral resolution was ± 75 cm^{-1}, and it is likely that C−H stretching vibrations of the alkane moiety of the dithiol linker would contribute to the measured CARS signal at 3000 cm^{-1}.

Conclusions

Multilayer nanoparticle arrays were synthesized by depositing gold nanoparticles onto silane derivatized microscope glass slides. Multiple layers of gold nanoparticles were deposited using a dithiol linker molecule. A Raman-active analyte, oxazine 720, was deposited on top of the nanostructured material, and the CARS signal was monitored as a function of the number of nanoparticle depositions. We have shown that for the oxazine signal at 1600 cm^{-1}, maximum enhancement of the CARS signal was observed for 11 nanoparticle depositions. In addition, the oxazine signal at 3000 cm^{-1} shows maximum CARS enhancement for 13 nanoparticle layers depositions. We attribute the CARS enhancement to the enhanced electromagnetic fields arising from surface plasmon excitation using pump or Stokes laser beams and/or the emitted anti-Stokes signal, depending on the location of the Stokes field frequency relative to the substrate surface plasmon resonance frequency. The second harmonic generation signal from the nanoparticle substrates was also examined and maximum enhancement was observed for 13 nanoparticle layers. These results demonstrate that one can tune the nanostructures substrates to yield maximum NLO response for either (or both) process(es) based on the number of nanoparticle depositions that are performed.

Acknowledgment. Funding from the Canada Foundation for Innovation, the British Columbia Knowledge Development Fund, the Natural Sciences and Engineering Research Council of Canada, and the University of Victoria through the New Opportunities Program is gratefully acknowledged. Instrumentation and infrastructure were provided by the UBC Laboratory for Advanced Spectroscopy and Imaging Research at UBC.

References and Notes

(1) Jain, P. K.; Lee, K. S.; El-Sayed, I. H.; El-Sayed, M. A. Calculated Absorption and Scattering Properties of Gold Nanoparticles of Different Size, Shape, and Composition: Applications in Biological Imaging and Biomedicine. *J. Phys. Chem. B* **2006**, *110* (14), 7238–7248.

(2) Lee, E.-H.; Park, K. Potential applications of nanoscale semiconductor quantum devices for information and telecommunications technologies. *Mater. Sci. Eng.* **2000**, *B74* (1−3), 1–6.

(3) Van der Boom, M. E. Nanostructured molecular materials for device-quality, highly efficient electrooptic poled polymers. *Angew. Chem., Int. Ed.* **2002**, *41* (18), 3363–3366.

(4) Brongersma, M. L. Nanoscale photonics: Nanoshells: gifts in a gold wrapper. *Nat. Mater.* **2003**, *2* (5), 296–297.

(5) Aroca, R., *Surface-enhanced vibrational spectroscopy*; John Wiley & Sons: New York, 2006.

(6) Brolo, A. G.; Irish, D. E.; Smith, B. D. Applications of SERS to the study of metal-adsorbate interactions. *J. Mol. Spectrosc.* **1997**, *405*, 29–44.

(7) Moskovits, M. SERS. *Rev. Mod. Phys.* **1985**, *57*, 783–826.

(8) Otto, A.; Mrozek, I.; Grabhorn, H.; Akemann, W. SERS. *J. Phys.: Condens. Matter* **1992**, *4*, 1143–1212.

(9) Schatz, G. C.; Duyne, R. P. V. EM mechanism of SERS. In *Handbook of Vibrational Spectroscopy*; Chalmers, J. M., Griffiths, P. R., Eds.; Wiley: New York, 2002.

(10) Constantino, C. J. L.; Lemma, T.; Antunes, P. A.; Aroca, R. Single molecule detection using SERRS and Langmuir Blodgett monolayers. *Anal. Chem.* **2001**, *73*, 3674–3678.

(11) Graham, D. Simple multiplex genotyping by SERS. *Anal. Chem.* **2002**, *74*, 1069–1074.

(12) Kneipp, K.; Kneipp, H.; Itzkan, I.; Dasari, R. R.; Feld, M. S. Ultrasensitive chemical analysis by Raman spectroscopy. *Chem. Rev.* **1999**, *99*, 2957–2975.

(13) Kneipp, K.; Kneipp, H.; Itzkan, I.; Dasari, R. R.; Feld, M. S. Ultrasensitive chemical analysis by Raman spectroscopy. *Chem. Rev.* **1999**, *99*, 2957–2975.

(14) Ataka, K.; Heberle, J. Biochemical applications of surface-enhanced infrared absorption spectroscopy. *Anal. Bioanal. Chem.* **2007**, *388* (1), 47–54.

(15) Aslan, K.; Lakowicz, J. R.; Geddes, C. D. Plasmon light scattering in biology and medicine: new sensing approaches, visions and perspectives. *Curr. Opin. Chem. Biol.* **2005**, *9* (5), 538–544.

(16) Agarwal, G. S.; Jha, S. S. Theory of second harmonic generation at a metal surface with surface plasmon excitation. *Solid State Commun.* **1982**, *41* (6), 499–501.

(17) Schatz, G. C.; Van Duyne, R. P., Electromagnetic Mechanism of Surface-enhanced Spectroscopy. In *Handbook of Vibrational Spectroscopy*; Chalmers, J. M.; Griffiths, P. R., Eds.; Johny Wiley & Sons Ltd.: Chichester, 2002; Vol. 1.

(18) McMahon, M. D.; Ferrara, D.; Bowie, C. T.; Lopez, R.; Haglund, R. F. Second harmonic generation from resonantly excited arrays of gold nanoparticles. *Appl. Phys. B* **2007**, *87* (2), 259–265.

(19) Chen, K.; Durak, C.; Heflin, J. R.; Robinson, H. D. Plasmon-enhanced second-harmonic generation from ionic self-assembled multilayer films. *Nano Lett.* **2007**, *7* (2), 254–258.

(20) Antoine, R.; Brevet, P. F.; Girault, H. H.; Bethell, D.; Schiffrin, D. J. Surface plasmon enhanced non-linear optical response of gold nanoparticles at the air/toluene interface. *Chem. Commun.* **1997**, (19), 1901–1902.

(21) Kim, E. M.; Elovikov, S. S.; Murzina, T. V.; Aktsipetrov, O. A.; Bader, M. A.; Marowsky, G. Giant third optical harmonic generation in island silver films. *Jet. Lett.* **2004**, *80* (8), 527–531.

(22) Lamprecht, B.; Krenn, J. R.; Leitner, A.; Aussenegg, F. R. Resonant and off-resonant light-driven plasmons in metal nanoparticles studied by femtosecond-resolution third-harmonic generation. *Phys. Rev. Lett.* **1999**, *83* (21), 4421–4424.

(23) Hayazawa, N.; Ichimura, T.; Hashimoto, M.; Inouye, Y.; Kawata, S. Amplification of coherent anti-Stokes Raman scattering by a metallic nanostructure for a high resolution vibration microscopy. *J. Appl. Phys.* **2004**, *95* (5), 2676–2681.

(24) Simon, H. J.; Andrews, J. R. Coherent Anti-Stokes Raman (Cars) Generation with Surface-Plasmons. *Bul. Am. Phys. Soc.* **1979**, *24* (3), 441–441.

(25) Muhlschlegel, P.; Eisler, H. J.; Martin, O. J. F.; Hecht, B.; Pohl, D. W. Resonant optical antennas. *Science* **2005**, *308* (5728), 1607–1609.

(26) Lyon, L. A.; Musick, M. D.; Natan, M. J. Colloidal Au-enhanced surface plasmon resonance immunosensing. *Anal. Chem.* **1998**, *70* (24), 5177–5183.

(27) Su, K. H.; Wei, Q. H.; Zhang, X.; Mock, J. J.; Smith, D. R.; Schultz, S. Interparticle Coupling Effects on Plasmon Resonances of Nanogold Particles. *Nano Lett.* **2003**, *3* (8), 1087–1090.

(28) Grabar, K. C.; Freeman, R. G.; Hommer, M. B.; Natan, M. J. Preparation and Characterization of Au Colloid Monolayers. *Anal. Chem.* **1995**, *67* (4), 735–43.

(29) Grabar, K. C.; Smith, P. C.; Musick, M. D.; Davis, J. A.; Walter, D. G.; Jackson, M. A.; Guthrie, A. P.; Natan, M. J. Kinetic Control of Interparticle Spacing in Au Colloid-Based Surfaces: Rational Nanometer-Scale Architecture. *J. Am. Chem. Soc.* **1996**, *118* (5), 1148–53.

(30) Link, S.; Mohamed, M. B.; El-Sayed, M. A. Simulation of the optical absorption spectra of gold nanorods as a function of their aspect ratio and the effect of the medium dielectric constant. *J. Phys. Chem. B* **1999**, *103* (16), 3073–3077.

(31) Sandrock, M. L.; Pibel, C. D.; Geiger, F. M.; Foss, C. A. Synthesis and second-harmonic generation studies of noncentrosymmetric gold nanostructures. *J. Phys. Chem. B* **1999**, *103* (14), 2668–2673.

(32) Hulteen, J. C. Nanofabricated surfaces: design, characterization by atomic force microscopy, and surface-enhanced spectroscopy of adsorbates (nanosphere lithography), 1995.

(33) Canfield, B. K.; Kujala, S.; Jefimovs, K.; Turunen, J.; Kauranen, M. Linear and nonlinear optical responses influenced by broken symmetry in an array of gold nanoparticles. *Opt. Exp.* **2004**, *12* (22), 5418–5423.

(34) Brolo, A. G.; Arctander, E.; Gordon, R.; Leathem, B.; Kavanagh, K. L. Nanohole-Enhanced Raman Scattering. *Nano Lett.* **2004**, *4* (10), 2015–2018.

(35) Canfield, B. K.; Kujala, S.; Jefimovs, K.; Vallius, T.; Turunen, J.; Kauranen, M. Polarization effects in the linear and nonlinear optical responses of gold nanoparticle arrays. *J. Opt. A* **2005**, *7* (2), S110–S117.

(36) Canfield, B. K.; Kujala, S.; Laiho, K.; Jefimovs, K.; Turunen, J.; Kauranen, M. Chirality arising from small defects in gold nanoparticle arrays. *Opt. Exp.* **2006**, *14* (2), 950–955.

(37) Canfield, B. K.; Kujala, S.; Laiho, K.; Jefimovs, K.; Vallius, T.; Turunen, J.; Kauranen, M. Linear and nonlinear optical properties of gold nanoparticles with broken symmetry. *J. Nonlinear Opt. Phys. Mater.* **2006**, *15* (1), 43–53.

(38) Addison, C. J.; Brolo, A. G. Nanoparticle-Containing Structures as a Substrate for Surface-Enhanced Raman Scattering. *Langmuir* **2006**, *22* (21), 8696–8702.

(39) Ulman, A. Formation and Structure of Self-Assembled Monolayers. *Chem. Rev.* **1996**, *96*, 1533–1554.

(40) Fan, M.; Brolo, A. G. Self-assembled Au nanoparticles as substrates for surface-enhanced vibrational spectroscopy: optimization and electrochemical stability. *Chem. Phys. Chem.* **2008**, *9* (13), 1899–1907.

(41) Brolo, A. G.; Germain, P.; Hager, G. Investigation of the Adsorption of L-Cysteine on a Polycrystalline Silver Electrode by Surface-Enhanced Raman Scattering (SERS) and Surface-Enhanced Second Harmonic Generation (SESHG). *J. Phys. Chem. B* **2002**, *106* (23), 5982–5987.

(42) Morita, S.; Wiesendanger, R.; Meyer, E. *Noncontact Atomic Force Microscopy*; Springer: 2002.

(43) Otto, A.; Mrozek, I.; Grabhorn, H.; Akemann, W. Surface-enhanced Raman scattering. *J. Phys.: Condens. Matter* **1992**, *4* (5), 1143–212.

(44) Lyon, L. A.; Keating, C. D.; Fox, A. P.; Baker, B. E.; He, L.; Nicewarner, S. R.; Mulvaney, S. P.; Natan, M. J. Raman Spectroscopy. *Anal. Chem.* **1998**, *70* (12), 341R–361R.

(45) Campion, A.; Kambhampati, P. Surface-enhanced Raman scattering. *Chem. Soc. Rev.* **1998**, *27* (4), 241–250.

(46) Doron, A.; Joselevich, E.; Schlittner, A.; Willner, I. AFM characterization of the structure of Au-colloid monolayers and their chemical etching. *Thin Solid Films* **1999**, *340* (1,2), 183–188.

(47) Canfield, B. K.; Husu, H.; Laukkanen, J.; Bai, B. F.; Kuittinen, M.; Turunen, J.; Kauranen, M. Local field asymmetry drives second-harmonic generation in noncentrosymmetric nanodimers. *Nano Lett.* **2007**, *7* (5), 1251–1255.

(48) Srinivasan, R.; Tian, Y.; Suni, I. I. Surface plasmon effects on surface second harmonic generation during Au nanoparticle deposition onto H-Si(1 1 1). *Surf. Sci.* **2001**, *490* (3), 308–314.

(49) Chen, C. K.; De Castro, A. R. B.; Shen, Y. R. Surface-enhanced second-harmonic generation. *Phys. Rev. Lett.* **1981**, *46* (2), 145–8.

(50) Wokaun, A.; Bergman, J. G.; Heritage, J. P.; Glass, A. M.; Liao, P. F.; Olson, D. H. Surface second-harmonic generation from metal island films and microlithographic structures. *Phys. Rev. B* **1981**, *24* (2), 849–56.

(51) Jin, R. C.; Jureller, J. E.; Kim, H. Y.; Scherer, N. F. Correlating second harmonic optical responses of single Ag nanoparticles with morphology. *J. Am. Chem. Soc.* **2005**, *127* (36), 12482–12483.

(52) Abid, J.-P.; Nappa, J.; Girault, H. H.; Brevet, P.-F. Pure surface plasmon resonance enhancement of the first hyperpolarizability of gold core-silver shell nanoparticles. *J. Chem. Phys.* **2004**, *121* (24), 12577–12582.

(53) Nappa, J.; Russier-Antoine, I.; Benichou, E.; Jonin, C.; Brevet, P. F. Second harmonic generation from small gold metallic particles: From the dipolar to the quadrupolar response. *J. Chem. Phys.* **2006**, *125* (18), .

(54) Kujala, S.; Canfield, B. K.; Kauranen, M.; Svirko, Y.; Turunen, J. Multipole interference in the second-harmonic optical radiation from gold nanoparticles. *Phys. Rev. Lett.* **2007**, *98* (16), .

(55) Kujala, S.; Canfield Brian, K.; Kauranen, M.; Svirko, Y.; Turunen, J. Multipolar analysis of second-harmonic radiation from gold nanoparticles. *Opt. Exp.* **2008**, *16* (22), 17196–208.

(56) Hubert, C.; Billot, L.; Adam, P. M.; Bachelot, R.; Royer, P.; Grand, J.; Gindre, D.; Dorkenoo, K. D.; Fort, A. Role of surface plasmon in second harmonic generation from gold nanorods. *Appl. Phys. Lett.* **2007**, *90* (18), 181105/1–181105/3.

(57) Gao, H. W.; Henzie, J.; Odom, T. W. Direct evidence for surface plasmon-mediated enhanced light transmission through metallic nanohole arrays. *Nano Lett.* **2006**, *6* (9), 2104–2108.

(58) Demtroder, W. *Laser Spectroscopy: Basic Concepts and Instrumentation*, 3rd ed.; Springer: New York, 2003; p 987.

(59) Chew, H.; Wang, D. S.; Kerker, M. Surface enhancement of coherent anti-Stokes Raman scattering by colloidal spheres. *J. Opt. Soc. Am. B* **1984**, *1* (1), 56–66.

(60) Liang, E. J.; Weippert, A.; Funk, J. M.; Materny, A.; Kiefer, W. Experimental observation of surface-enhanced coherent anti-Stokes Raman scattering. *Chem. Phys. Lett.* **1994**, *227* (1−2), 115–20.

(61) Ichimura, T.; Hayazawa, N.; Hashimoto, M.; Inouye, Y.; Kawata, S. Local enhancement of coherent anti-Stokes Raman scattering by isolated gold nanoparticles. *J. Raman Spectrosc.* **2003**, *34* (9), 651–654.

(62) Okamoto, T.; Yamaguchi, I. Optical Absorption Study of the Surface Plasmon Resonance in Gold Nanoparticles Immobilized onto a Gold Substrate by Self-Assembly Technique. *J. Phys. Chem. B* **2003**, *107* (38), 10321–10324.

(63) Bright, R. M.; Musick, M. D.; Natan, M. J. Preparation and Characterization of Ag Colloid Monolayers. *Langmuir* **1998**, *14* (20), 5695–5701.

(64) Musick, M. D.; Keating, C. D.; Lyon, L. A.; Botsko, S. L.; Pena, D. J.; Holliway, W. D.; McEvoy, T. M.; Richardson, J. N.; Natan, M. J. Metal Films Prepared by Stepwise Assembly. 2. Construction and Characterization of Colloidal Au and Ag Multilayers. *Chem. Mater.* **2000**, *12* (10), 2869–2881.

(65) Olson, L. G.; Lo, Y.-S.; Beebe, T. P., Jr.; Harris, J. M. Characterization of Silane-Modified Immobilized Gold Colloids as a Substrate for Surface-Enhanced Raman Spectroscopy. *Anal. Chem.* **2001**, *73* (17), 4268–4276.

(66) McFarland, A. D.; Young, M. A.; Dieringer, J. A.; Van Duyne, R. P. Wavelength-Scanned Surface-Enhanced Raman Excitation Spectroscopy. *J. Phys. Chem. B* **2005**, *109* (22), 11279–11285.

(67) Etchegoin, P.; Cohen, L. F.; Hartigan, H.; Brown, R. J. C.; Milton, M. J. T.; Gallop, J. C. Electromagnetic contribution to surface enhanced Raman scattering revisited. *J. Chem. Phys.* **2003**, *119* (10), 5281–5289.

(68) Etchegoin, P.; Liem, H.; Maher, R. C.; Cohen, L. F.; Brown, R. J. C.; Milton, M. J. T.; Gallop, J. C. Observation of dynamic oxygen release in hemoglobin using surface enhanced Raman scattering. *Chem. Phys. Lett.* **2003**, *367* (1−2), 223–229.

JP809579B